












Spin-wave eigenmodes in direct-write 3D nanovolcanoes

Cite as: Appl. Phys. Lett. **118**, 132405 (2021); <https://doi.org/10.1063/5.0044325>

Submitted: 15 January 2021 . Accepted: 14 March 2021 . Published Online: 30 March 2021

 O. V. Dobrovolskiy,  N. R. Vovk,  A. V. Bondarenko,  S. A. Bunyaev,  S. Lamb-Camarena,  N. Zenbaa, R. Sachser,  S. Barth,  K. Y. Guslienko,  A. V. Chumak,  M. Huth,  G. N. Kakazei, et al.

COLLECTIONS

Paper published as part of the special topic on [Mesoscopic Magnetic Systems: From Fundamental Properties to Devices](#)



View Online



Export Citation



CrossMark

ARTICLES YOU MAY BE INTERESTED IN

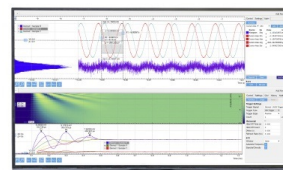
[Long-range spin-wave propagation in transversely magnetized nano-scaled conduits](#)
Applied Physics Letters **118**, 132406 (2021); <https://doi.org/10.1063/5.0045570>

[Engineered magnetization and exchange stiffness in direct-write Co-Fe nanoelements](#)
Applied Physics Letters **118**, 022408 (2021); <https://doi.org/10.1063/5.0036361>

[Introduction to spin wave computing](#)
Journal of Applied Physics **128**, 161101 (2020); <https://doi.org/10.1063/5.0019328>

Challenge us.

What are your needs for periodic signal detection?



Zurich Instruments

Spin-wave eigenmodes in direct-write 3D nanovolcanoes

Cite as: Appl. Phys. Lett. **118**, 132405 (2021); doi: [10.1063/5.0044325](https://doi.org/10.1063/5.0044325)

Submitted: 15 January 2021 · Accepted: 14 March 2021 ·

Published Online: 30 March 2021



View Online



Export Citation



CrossMark

O. V. Dobrovolskiy,^{1,a)} N. R. Vovk,^{2,3} A. V. Bondarenko,² S. A. Bunyaev,² S. Lamb-Camarena,¹ N. Zenbaa,¹ R. Sachser,⁴ S. Barth,⁴ K. Y. Guslienko,^{5,6} A. V. Chumak,¹ M. Huth,⁴ and G. N. Kakazei²

AFFILIATIONS

¹Faculty of Physics, University of Vienna, 1090 Vienna, Austria

²Institute of Physics for Advanced Materials, Nanotechnology and Photonics (IFIMUP)/Departamento de Física e Astronomia, Universidade do Porto, 4169-007 Porto, Portugal

³Department of Physics, V. N. Karazin Kharkiv National University, Svobody Sq. 4, Kharkiv 61022, Ukraine

⁴Physikalisches Institut, Goethe University, 60438 Frankfurt am Main, Germany

⁵Division de Física de Materiales, Depto. Polímeros y Materiales Avanzados: Física, Química y Tecnología, Universidad del País Vasco, UPV/EHU, 20018 San Sebastian, Spain

⁶IKERBASQUE, the Basque Foundation for Science, 48009 Bilbao, Spain

Note: This paper is part of the APL Special Collection on Mesoscopic Magnetic Systems: From Fundamental Properties to Devices.

a) Author to whom correspondence should be addressed: oleksandr.dobrovolskiy@univie.ac.at

ABSTRACT

Extending nanostructures into the third dimension has become a major research avenue in modern magnetism, superconductivity, and spintronics, because of geometry-, curvature-, and topology-induced phenomena. Here, we introduce Co-Fe nanovolcanoes—nanodisks overlaid by nanorings—as purpose-engineered 3D architectures for nanomagnonics, fabricated by focused electron beam-induced deposition. We use both perpendicular spin-wave resonance measurements and micromagnetic simulations to demonstrate that the rings encircling the volcano craters harbor the highest-frequency eigenmodes, while the lower-frequency eigenmodes are concentrated within the volcano crater, due to the non-uniformity of the internal magnetic field. By varying the crater diameter, we demonstrate the deliberate tuning of higher-frequency eigenmodes without affecting the lowest-frequency mode. Thereby, the extension of 2D nanodisks into the third dimension allows one to engineer their lowest eigenfrequency by using 3D nanovolcanoes with 30% smaller footprints. The presented nanovolcanoes can be viewed as multi-mode microwave resonators and 3D building blocks for nanomagnonics.

© 2021 Author(s). All article content, except where otherwise noted, is licensed under a Creative Commons Attribution (CC BY) license (<http://creativecommons.org/licenses/by/4.0/>). <https://doi.org/10.1063/5.0044325>

Extending nanomagnets into the third dimension has become a vibrant research avenue in modern magnetism.^{1,2} It encompasses investigations of 3D frustrated systems,^{3–6} topology- and curvature-induced effects in complex-shaped nano-architectures,^{7–10} and the dynamics of spin waves in 3D magnonic systems.^{11–15} In magnonics, which is concerned with the operations with data carried by spin waves, magnonic conduits have traditionally been made from 2D structures.^{16–21} Extension of spin-wave circuits into the third dimension is required for the reduction of footprints of magnonic logic gates,²⁰ and it allows, e.g., steering of spin-wave beams in graded-index magnonics.^{22–24} In addition, the height of nanomagnets offers an additional degree of freedom in the rapidly developing domain of inverse-design magnonics^{25,26} in which a device functionality is first

specified and then a feedback-based computational algorithm is used to obtain the device design. In the past, peculiarities of the lithographic process were used, e.g., for the formation of crowns on the tops of nanodisks.²⁷ However, lithographic techniques insufficiently suit the demands of 3D magnonics. This motivates the increasingly growing attention to additive manufacturing nanotechnologies.²

In recent years, two-photon 3D lithography and 3D direct writing by focused electron and ion beam-induced deposition (FEBID and FIBID) have become the techniques of choice for the fabrication of complex-shaped nano-architectures in magnetism, superconductivity, and plasmonics.^{2–4,9,28–33} For magnonics, the propagation of spin waves in direct-write Fe- and Co-based conduits has recently been demonstrated, with a spin-wave decay length in the range of

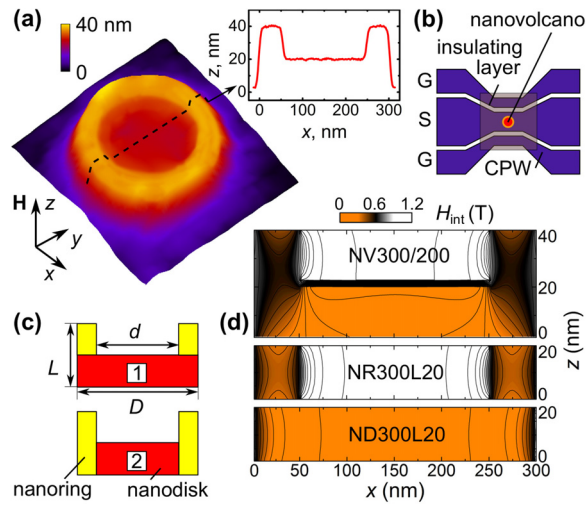


FIG. 1. Experimental geometry. (a) Atomic force microscopy image of the nanovolcano NV300/200 with the outer diameter of $D = 300$ nm and the crater diameter of $d = 200$ nm. Inset: cross-sectional line scan, as indicated. (b) Active part of the coplanar waveguide (S: signal; G: ground) with a nanovolcano for microwave spectroscopy measurements (not to scale). (c) Possible ways of splitting a nanovolcano into a combination of a disk and a ring for modeling. (d) Calculated spatial dependence of the internal field H_{int} for the 40 nm-thick nanovolcano NV300/200 and its individual basic elements (nanodisk ND300L20 and nanoring NR300L20) at the out-of-plane bias magnetic field of $H = 1.2$ T.

3–6 μm .^{34,35} Given FEBID’s lateral resolution down to 10 nm and its versatility regarding the substrate material, FEBID appears as a promising nanofabrication technology for 3D magnonics.³⁶

Here, we investigate the spin-wave eigenmodes in individual direct-write Co-Fe nanovolcanoes by spin-wave resonance (SWR) spectroscopy^{37,38} and analyze the experimental data with the aid of micromagnetic simulations. We reveal that the microwave response of the nanovolcanoes essentially differs from the sum of the microwave responses of their constituent 2D elements—nanorings and nanodisks.

TABLE I. Sample parameters and simulated SWR frequencies for nano-volcanoes, nano-rings, and nano-disks. NV: nanovolcano; ND: nanodisk; NR: nanoring; D : outer diameter; d : inner diameter; L : thickness; M_s : saturation magnetization; A : exchange stiffness. M_s and A values correspond to those for equivalent diameter Co-Fe nanodisks.³⁷ The frequencies of the modes D1–D3, R1, and R2 are calculated at 1.7 T for NV1000/700 and NV600/400 and at 1.2 T for all other samples. Upper part: Nanovolcanoes studied experimentally and by micromagnetic simulations. Lower part: Nanovolcanoes’ individual elements (nanodisks and nanorings) studied by simulations.

Sample	D/d , nm	L , nm	M_s , kA/m	A , pJ/m	D1, GHz	D2, GHz	D3, GHz	R1, GHz	R2, GHz
NV1000/700		40	1125	16.7	10.19	11.70	13.11	20.22	21.05
NV600/400		40	1030	16.1	14.57	17.04	19.04	26.93	28.58
NV300/180		40	880	15.4	7.29	12.06	17.85	22.01	23.66
NV300/200		40	880	15.4	7.32	11.67	17.01	21.95	25.16
NV300/220		40	880	15.4	7.38	11.37	16.25	25.95	27.71
NR300/200		20	880	15.4	17.72
NR300/200		40	880	15.4	24.89
ND200		20	880	15.4	10.47	15.83	21.68
ND300		20	880	15.4	7.92	11.37	15.05
ND340		20	880	15.4	7.32	10.44	13.65

We demonstrate that the ring encircling the volcano crater leads to an effective confinement of the low-frequency eigenmodes under the volcano crater, while the higher-frequency eigenmodes are confined in the ring area. By varying the crater diameter by ± 20 nm, we demonstrate the deliberate tuning of the higher eigenfrequencies by about ± 2 GHz without essential variation of the lowest eigenfrequency. The presented nanovolcanoes can be viewed as multi-mode resonators and as 3D building blocks for nanomagnonics.

The 40 nm-thick Co-Fe nanovolcanoes with diameters down to 300 nm and crater diameters down to 180 nm were fabricated by FEBID (SEM: FEI Nova NanoLab 600) on top of a gold coplanar waveguide (CPW) (see Fig. 1). FEBID was performed with 5 kV/1.6 nA, a pitch of 20 nm, a dwell time of 1 μs , $\text{HCo}_3\text{Fe}(\text{CO})_{12}$ as precursor gas,^{39,40} and a serpentine scanning strategy.³⁸ For the experiments discussed in what follows, we selected, by atomic force microscopy (AFM) inspection, five nano-volcanoes with the outer and inner (crater) diameters, D and d , respectively, deviating by less than ± 3 nm from the nominal values reported in Table I. We label the nanovolcanoes with their diameter ratios NVD/d (omitting the units “nm”) and use the prefixes ND and NR for the nanodisks and nanorings. These simpler objects, investigated extensively in the past,^{41–47} can be naively viewed as constituent elements of the nanovolcanoes [see Fig. 1(c)]. All nanovolcanoes exhibit a flat morphology and a slightly trapezoidal cross-sectional profile, as revealed by atomic force microscopy [see Fig. 1(a)].

The CPWs were prepared by e-beam lithography from a 55 nm-thick Au film sputtered onto a Si/SiO₂ (200 nm) substrate with a 5 nm-thick Cr buffer layer. The CPWs were covered with a 5 nm-thick TiO₂ layer (e-beam lithography) for electrical insulation from the nanovolcanoes. The width and length of the narrowed middle part of the CPW signal line [see Fig. 1(b)] were equal to $2D$ and $4D$ of the nanovolcano under study, respectively [see Fig. 1(b)]. SWR measurements were taken in the frequency range of 4–32 GHz with a bias magnetic field in the range of 1.2–2 T, oriented perpendicular to the volcano plane. The field alignment error was less than 0.1° , which is too small to cause splitting of spin-wave modes in perpendicularly magnetized nanostructures.⁴⁸ The high-frequency ac excitation was

provided by a microwave generator, and the transmitted signal was detected using a signal analyzer. The measurements were performed with a bias magnetic field modulation amplitude of 1 mT, a frequency of 15 Hz, and a phase-sensitive recording of the microwave transmission.

Figures 2(a) and 2(b) present the experimentally measured microwave power absorption spectra for the nanovolcanoes NV300/200 and NV300/220 at 1.2 T. For both nanovolcanoes, the spectra contain the dominating low-frequency SWR modes (D1) at about 7.35 GHz and the pronounced higher-frequency SWR modes (R1 and R2). The increase in the crater diameter d from 180 nm to 220 nm leads to a blue shift of the R1 and R2 peaks by about 4 GHz (see also Table I). Interestingly, these changes in the high-frequency part of the spectrum are accompanied by the opposite (though much weaker) shifts of the lower eigenfrequencies (D_2 , D_3) and a nearly constant eigenfrequency D_1 , as shown in Fig. 2(c).

To identify the SWR modes associated with different parts of the nanovolcanoes, micromagnetic simulations were performed using the MuMax3 solver.⁴⁹ For all nanovolcanoes, the cell size was $2.5 \times 2.5 \times 2.5 \text{ nm}^3$ and the damping parameter was $\alpha = 0.01$. The simulations were performed in two stages. First, an equilibrium magnetic configuration of the system was reached by relaxing a random magnetic configuration for a given perpendicular bias field value. Subsequently, magnetization precession was excited by applying a small spatially uniform in-plane microwave field pulse. Finally, a fast Fourier transform was used to extract the normalized frequency spectra and the spatial dependences of the spin-wave eigenmodes. In the

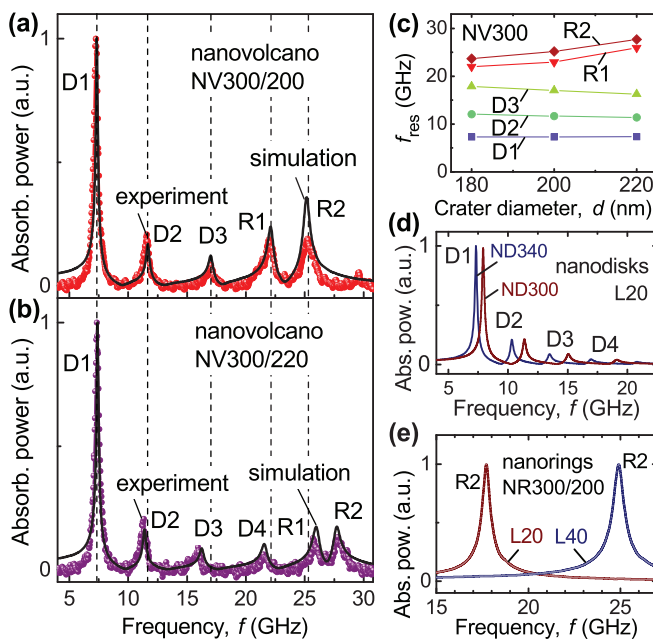


FIG. 2. Measured (symbols) and calculated (lines) power absorption spectra for the nanovolcanoes (a) NV300/200 and (b) NV300/220. (c) Experimentally deduced resonance frequencies f_{res} vs crater diameter d for the nanovolcanoes with $D = 300 \text{ nm}$. Calculated power absorption spectra for (d) the nanodisks with a thickness of $L = 20 \text{ nm}$ and diameters of $D = 300 \text{ nm}$ and 340 nm and (e) the nanorings NR300/200 with thicknesses of $L = 20 \text{ nm}$ and 40 nm . In all panels, $H = 1.2 \text{ T}$.

simulations, we used the saturation magnetization M_s and exchange stiffness A values deduced for the disks with the same diameters and deposited with the same FEBID parameters³⁷ (Table I) and the assumed gyromagnetic ratio of $\gamma/2\pi = 3.05 \text{ MHz/Oe}$.⁵⁰ The decrease in M_s and A with the decrease in the disk diameter from $1 \mu\text{m}$ to 300 nm is associated with a decrease in the $[\text{Co}_3\text{Fe}]$ content from $80 \pm 3 \text{ at. \%}$ to $63 \pm 3 \text{ at. \%}$ and an increase in the $[\text{C} + \text{O}]$ content from $20 \pm 3 \text{ at. \%}$ to $37 \pm 3 \text{ at. \%}$ (as residues from the precursor in the FEBID process).³⁷

The calculated microwave absorption spectra for the nanovolcanoes NV300/200 and NV300/220 are shown by solid lines in Figs. 2(a) and 2(b). The calculated spectra fit well with the experimentally measured ones. With the increase in diameter d , the R1 and R2 modes are shifted by a few GHz toward higher frequencies. The increase in d has a very weak influence on the location of the SWR modes D1–D3. Observation of the enhancements afforded by the 3D extrusion in comparison to a pure nanodisk geometry is possible if one takes a naive view of a nanovolcano as a composite geometrical object composed of a 20 nm-thick nanodisk overlaid by a 20 nm-thick nanoring [geometry 1 in Fig. 1(c)]. The simulations predict the lowest-frequency mode for the nanodisk ND300 at a frequency f_{res} of 7.9 GHz [Fig. 2(d)], which is about 600 MHz above the experimentally measured value for the equivalent diameter nanovolcano, NV300/200. In contrast, the calculated f_{res} of the 20 nm-thick nanodisk ND340, which has a larger diameter of 340 nm, matches well with the experimentally measured $f_{\text{res}} = 7.32 \text{ GHz}$ of the NV300/200 nanovolcano. This is to say that the lowest-frequency eigenmode of a model nanovolcano, i.e., a 20 nm-thick disk (volcano basement) overlaid by a 20 nm-thick ring, can be obtained in simulations for a 20 nm-thick disk, which has a larger effective diameter $D_{\text{eff}} = 340 \text{ nm}$. That is, extension of a 2D nanomagnet into the third dimension allows one to engineer the lowest eigenfrequency of a nanodisk by using a 3D nanovolcano, which has an about 30% smaller footprint. This phenomenon will be discussed below.

We have also calculated f_{res} for 20 nm- and 40 nm-thick nanorings NR300/200 at 1.2 T [Fig. 2(e)]. For the 20 nm-thick nanoring NR300/200 [geometry 1 in Fig. 1(c)], $f_{\text{res}} = 17.75 \text{ GHz}$ is very far away from modes R1 (22.02 GHz) and R2 (25.15 GHz) of the equivalently sized nanovolcano NV300/200. This is because of the essentially larger internal field in the volcano's ring area as compared to the 20 nm-thick ring [Fig. 1(d)]. By contrast, for the 40 nm-thick nanoring NR300/200 nm at 1.2 T [geometry 2 in Fig. 1(c)], $f_{\text{res}} = 24.9 \text{ GHz}$ is very close to the measured R2 eigenfrequency (25.1 GHz) of the equivalently sized nanovolcano NV300/200 nm. In this way, the R2 peak can be ascribed to the ring mode of a nanoring with the same thickness as the nanovolcano and the width equal to that of the ring encircling the nanovolcano crater [geometry 2 in Fig. 1(c)].

The calculated spatial dependences of the spin-wave eigenmodes for the nanovolcano NV300/200 [Fig. 2(b)] are shown in Fig. 3(a). At first glance, the eigenmodes in the nanovolcano resemble spin-wave “drum modes” known for nanodisks saturated in the perpendicular geometry.^{37,41} These drum modes are approximately described by Bessel functions of the zeroth order⁴¹ and are shown in Fig. 3(b) for the 20 nm-thick nanodisk ND300 for comparison. This explains why the volcano low-frequency modes only weakly depend on the crater diameter [see Fig. 2(c)]. Indeed, a closer look at the D1–D3 mode profiles reveals that spin waves in the nanovolcano are confined under the

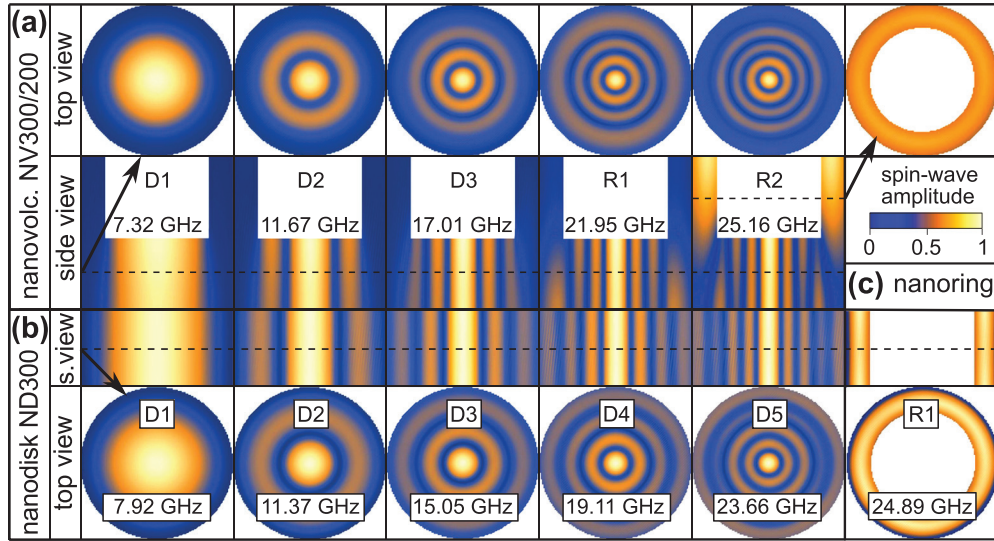


FIG. 3. Calculated spatial dependences of the spin-wave eigenfunctions for (a) the 40 nm-thick nanovolcano NV300/200, (b) the 20 nm-thick nanodisk ND300, and (c) the 20 nm-thick nanoring NR300/200 at the out-of-plane bias magnetic field of 1.2 T. The SWR modes correspond to those shown in Figs. 2(a), 2(d), and 2(e). The mutual relation between the cross-sectional profiles is indicated by the dashed lines.

volcano crater, which acts as a “concentrator” for spin waves. As it was mentioned earlier, the D1 mode frequency for NV300/200 is lower than that for ND300, while for higher frequency modes D2 and D3, the opposite behavior is observed. The following qualitative explanation of this effect can be proposed. (i) The internal field increases at the NV edge, and therefore, the D modes are pushed away from this region (i.e., toward the volcano center). As a result, the stronger confinement of the spin waves leads to an increase in their frequencies. This increase becomes more significant for higher mode numbers since the spin-wave frequency is approximately proportional to the square of the wavevector. (ii) In the NV300/200 center region, the internal field is slightly smaller than that in ND300, which results in a redshift of the D1 frequency. (iii) The effect of the reduced internal field is dominant for the D1 mode, resulting in its frequency redshift. On the contrary, the effect of confinement is dominant for the higher modes D2 and D3, resulting in their frequency blueshifts. The role of the ring overlying the volcano basement disk becomes more decisive for higher-frequency R eigenmodes. This can also be explained by the fact that the reduced effective width (proportional to the width $(D - d)/2$ of the ring) becomes more relevant for shorter wavelengths. The exchange interaction for the rings with widths ≈ 50 nm essentially contributes to the R2 frequency (the exchange length⁵¹ $\lambda = \sqrt{2A/(\mu_0 M_s^2)}$ in Co-Fe-FEBID is about 5 nm). Accordingly, the localization of the R2 mode in the ring is not a result of the reduced dipolar pinning,⁵² but is rather a result of the interplay of the exchange and internal magnetic fields.

Finally, with the increase in the nanovolcano diameter D , the number of SWR modes per given frequency interval increases (see Fig. 4). This can be understood as a reduction in the system sizes that leads to a stronger confinement of spin waves and the associated larger mode separation in the magnon frequency spectrum. With the increase in the magnetic field, the spectra are shifted toward higher frequencies as a whole, without qualitative changes in the structure of the

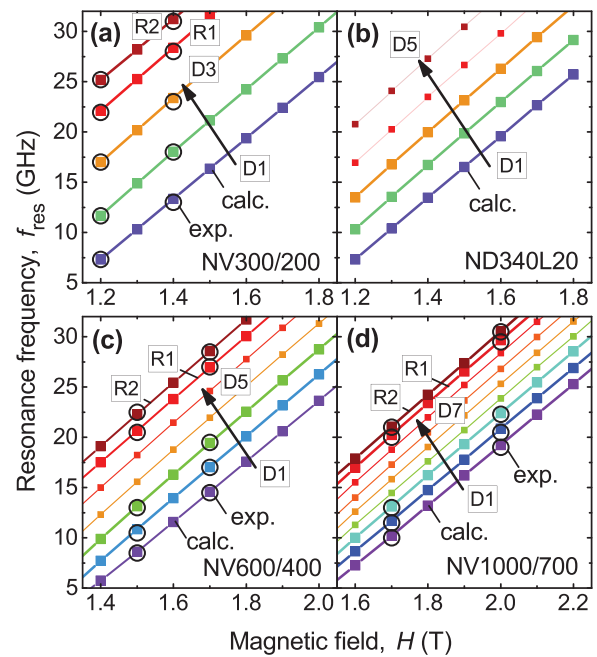


FIG. 4. Resonance frequencies vs bias magnetic field as deduced from SWR measurements (circles) and calculated numerically (squares) for (a) nanovolcano NV300/220, (b) nanodisk ND340L20, (c) nanovolcano NV600/400, and (d) nanovolcano NV1000/700. The dominating modes are indicated with larger symbols and thicker lines. The slope of straight lines is determined by $\gamma/2\pi = 3.05$ MHz/Oe.

spectra and the relative positions of the peaks. This can be understood on the basis of the nearly linear dependence $f_{\text{res}}(H) \simeq (\gamma/2\pi)H$ for axially symmetric nanoelements magnetized along the symmetry axis.⁴¹ The slope of all straight lines $f_{\text{res}}(H)$ in Fig. 4 is the same, and it is determined by the gyromagnetic ratio $\gamma/2\pi$.

To summarize, we have introduced nanovolcanoes as on-demand engineered nano-architectures for 3D magnetism and magnon spintronics. The 40 nm-thick Co-Fe nanovolcanoes with diameters down to 300 nm were fabricated by the direct-write FEBID technique and studied by perpendicular SWR spectroscopy. The spin-wave eigenfrequencies of the nanovolcanoes have been demonstrated to notably differ from the eigenfrequencies of the nanodisks and nanorings they are built from, because of the strongly non-uniform internal magnetic field. The experimental findings were elucidated with the aid of micromagnetic simulations, which indicate that the rings encircling the volcano craters lead to an effective confinement of the lower-frequency eigenmodes under the volcano crater, while the highest-frequency eigenmodes are confined in the ring area. Accordingly, extension of 2D nanodisks into the third dimension allows one to engineer their lowest eigenfrequencies by using 3D nanovolcanoes having about 30% smaller footprints. By varying the crater diameter by ± 20 nm, we have demonstrated a frequency tuning of about ± 2 GHz for the ring modes without affecting the lowest spin-wave eigenfrequency. The presented nanovolcanoes can be viewed as multi-mode resonators with potential applications in telecom-frequency filters. In addition, the engineered spin-wave frequency spectra make them prospective platforms for 3D magnonics and inverse-design magnonic devices.

O.V.D. and S.L.C. acknowledge the Austrian Science Fund (FWF) for support through Grant No. I 4889 (CurviMag). The Portuguese team acknowledges the Network of Extreme Conditions Laboratories-NECL and the Portuguese Foundation of Science and Technology (FCT) support through Project Nos. NORTE-01-0145-FEDER-022096, PTDC/FIS-MAC/31302/2017, POCI-0145-FEDER-030085 (NOVAMAG), and EXPL/IF/00541/2015. N. Z. and A. V. C. acknowledge the Austrian Science Fund (FWF) for support through Grant No. I 4917. S. B. acknowledges funding by the Deutsche Forschungsgemeinschaft (DFG) through Grant Nos. BA 6595/2-1 and BA 6595/1-1. K. G. acknowledges support from IKERBASQUE (the Basque Foundation for Science). The work of K. G. was supported by the Spanish Ministry of Science and Innovation through Grant No. PID2019-108075RB-C33/AEI/10.13039/501100011033. M.H. acknowledges the DFG for support through Grant No. HU 752/16-1. Support through the Frankfurt Center of Electron Microscopy (FCEM) is gratefully acknowledged. Further, support of the European Cooperation in Science and Technology via COST Action No. CA16218 (NANOCOHYBRI) is acknowledged.

DATA AVAILABILITY

The data that support the findings of this study are available within this article.

REFERENCES

¹A. Fernández-Pacheco, R. Streubel, O. Fruchart, R. Hertel, P. Fischer, and R. P. Cowburn, *Nat. Commun.* **8**, 15756 EP (2017).

- ²A. Fernández-Pacheco, L. Skoric, J. De Teresa, J. Pablo-Navarro, M. Huth, and O. V. Dobrovolskiy, *Materials* **13**, 3774 (2020).
- ³L. Keller, M. K. I. Al Mamoori, J. Pieper, C. Gspan, I. Stockem, C. Schröder, S. Barth, R. Winkler, H. Plank, M. Pohlit, J. Müller, and M. Huth, *Sci. Rep.* **8**, 6160 (2018).
- ⁴A. May, M. Hunt, A. Van Den Berg, A. Hejazi, and S. Ladak, *Commun. Phys.* **2**, 13 (2019).
- ⁵S. Gliga, E. Iacocca, and O. G. Heinonen, *APL Mater.* **8**, 040911 (2020).
- ⁶S. H. Skjærvø, C. H. Marrows, R. L. Stamps, and L. J. Heyderman, *Nat. Rev. Phys.* **2**, 13 (2020).
- ⁷R. Streubel, P. Fischer, F. Kronast, V. P. Kravchuk, D. D. Sheka, Y. Gaididei, O. G. Schmidt, and D. Makarov, *J. Phys. D* **49**, 363001 (2016).
- ⁸O. M. Volkov, A. Kákay, F. Kronast, I. Mönch, M.-A. Mawass, J. Fassbender, and D. Makarov, *Phys. Rev. Lett.* **123**, 077201 (2019).
- ⁹D. Sanz-Hernández, A. Hierro-Rodríguez, C. Donnelly, J. Pablo-Navarro, A. Sorrentino, E. Pereiro, C. Magén, S. McVitie, J. M. de Teresa, S. Ferrer, P. Fischer, and A. Fernández-Pacheco, *ACS Nano* **14**, 8084 (2020).
- ¹⁰D. D. Sheka, O. V. Pylypovskyi, P. Landeros, Y. Gaididei, A. Kákay, and D. Makarov, *Commun. Phys.* **3**, 128 (2020).
- ¹¹M. Krawczyk and H. Puzkarski, *Phys. Rev. B* **77**, 054437 (2008).
- ¹²M. Yan, C. Andreas, A. Kakay, F. Garcia-Sanchez, and R. Hertel, *Appl. Phys. Lett.* **99**, 122505 (2011).
- ¹³J. A. Otálora, M. Yan, H. Schultheiss, R. Hertel, and A. Kákay, *Phys. Rev. Lett.* **117**, 227203 (2016).
- ¹⁴*Three-Dimensional Magnonics: Layered, Micro- and Nanostructures*, edited by G. Gubbiotti (Jenny Stanford Publishing, 2019).
- ¹⁵V. K. Sakharov, E. N. Beginin, Y. V. Khivintsev, A. V. Sadovnikov, A. I. Stognij, Y. A. Filimonov, and S. A. Nikitov, *Appl. Phys. Lett.* **117**, 022403 (2020).
- ¹⁶V. V. Kruglyak, S. O. Demokritov, and D. Grundler, *J. Phys. D* **43**, 264001 (2010).
- ¹⁷*Magnonics*, edited by S. O. Demokritov and A. N. Slavin (Springer Berlin Heidelberg, 2013).
- ¹⁸X. M. Liu, J. Ding, G. N. Kakazei, and A. O. Adeyeye, *Appl. Phys. Lett.* **103**, 062401 (2013).
- ¹⁹G. N. Kakazei, X. M. Liu, J. Ding, and A. O. Adeyeye, *Appl. Phys. Lett.* **104**, 042403 (2014).
- ²⁰Q. Wang, M. Kewenig, M. Schneider, R. Verba, F. Kohl, B. Heinz, M. Geilen, M. Mohseni, B. Lägler, F. Ciubotaru, C. Adelman, C. Dubs, S. D. Cotozana, O. V. Dobrovolskiy, T. Brächer, P. Pirro, and A. V. Chumak, *Nat. Electron.* **3**, 765 (2020).
- ²¹Y. Li, W. Zhang, V. Tyberkevych, W.-K. Kwok, A. Hoffmann, and V. Novosad, *J. Appl. Phys.* **128**, 130902 (2020).
- ²²C. S. Davies, A. Francis, A. V. Sadovnikov, S. V. Chertopalov, M. T. Bryan, S. V. Grishin, D. A. Allwood, Y. P. Sharaevskii, S. A. Nikitov, and V. V. Kruglyak, *Phys. Rev. B* **92**, 020408 (2015).
- ²³J.-N. Toedt, M. Mundkowsky, D. Heitmann, S. Mendach, and W. Hansen, *Sci. Rep.* **6**, 33169 (2016).
- ²⁴P. Graczyk, J. Klos, and M. Krawczyk, *Phys. Rev. B* **95**, 104425 (2017).
- ²⁵Q. Wang, A. V. Chumak, and P. Pirro, *arXiv:2012.04544* (2020).
- ²⁶A. Papp, W. Porod, and G. Csaba, *arXiv:2012.04594*.
- ²⁷M. E. Steblii, A. V. Ognev, A. S. Samardak, A. Nogaret, and L. A. Chebotkevich, *Bull. Russ. Acad. Sci.* **75**, 193 (2011).
- ²⁸R. Winkler, F.-P. Schmidt, U. Haselmann, J. D. Fowlkes, B. B. Lewis, G. Kothleitner, P. D. Rack, and H. Plank, *ACS Appl. Mater. Interfaces* **9**, 8233 (2017).
- ²⁹O. V. Dobrovolskiy, V. M. Bezv, M. Y. Mikhailov, O. I. Yuzepovich, V. A. Shklovskij, R. V. Vovk, M. I. Tsindlekt, R. Sachser, and M. Huth, *Nat. Commun.* **9**, 4927 (2018).
- ³⁰R. Córdoba, D. Mailly, R. O. Rezaev, E. I. Smirnova, O. G. Schmidt, V. M. Fomin, U. Zeitler, I. Guillamón, H. Suderow, and J. M. De Teresa, *Nano Lett.* **19**, 8597 (2019).
- ³¹F. Porrati, S. Barth, R. Sachser, O. V. Dobrovolskiy, A. Seybert, A. S. Frangakis, and M. Huth, *ACS Nano* **13**, 6287 (2019).
- ³²R. Winkler, J. D. Fowlkes, P. D. Rack, and H. Plank, *J. Appl. Phys.* **125**, 210901 (2019).
- ³³O. V. Dobrovolskiy, V. M. Bezv, E. Begun, R. Sachser, R. V. Vovk, and M. Huth, *Phys. Rev. Appl.* **11**, 054064 (2019).

- ³⁴O. V. Dobrovolskiy, R. Sachser, S. A. Bunyaev, D. Navas, V. M. Bezv, M. Zeleny, W. Smigaj, J. Rychly, M. Krawczyk, R. V. Vovk, M. Huth, and G. N. Kakazei, *ACS Appl. Mater. Interfaces* **11**, 17654 (2019).
- ³⁵L. Flajšman, K. Wagner, M. Vaňatka, J. Gloss, V. Křížáková, M. Schmid, H. Schultheiss, and M. Urbánek, *Phys. Rev. B* **101**, 014436 (2020).
- ³⁶B. Dieny, I. L. Prejbeanu, K. Garello, P. Gambardella, P. Freitas, R. Lehndorff, W. Raberg, U. Ebels, S. O. Demokritov, J. Akerman, A. Deac, P. Pirro, C. Adelmann, A. Anane, A. V. Chumak, A. Hirohata, S. Mangin, S. O. Valenzuela, M. C. Onbaşlı, i. M. d'Aquino, G. Prenat, G. Finocchio, L. Lopez-Diaz, R. Chantrell, O. Chubykalo-Fesenko, and P. Bortolotti, *Nat. Electron.* **3**, 446 (2020).
- ³⁷O. V. Dobrovolskiy, S. A. Bunyaev, N. R. Vovk, D. Navas, P. Gruszecki, M. Krawczyk, R. Sachser, M. Huth, A. V. Chumak, K. Y. Guslienko, and G. N. Kakazei, *Nanoscale* **12**, 21207 (2020).
- ³⁸S. A. Bunyaev, B. Budinska, R. Sachser, Q. Wang, K. Levchenko, S. Knauer, A. V. Bondarenko, M. Urbanek, K. Y. Guslienko, A. V. Chumak, M. Huth, G. N. Kakazei, and O. V. Dobrovolskiy, *Appl. Phys. Lett.* **118**, 022408 (2021).
- ³⁹F. Porzati, M. Pohlit, J. Müller, S. Barth, F. Biegger, C. Gspan, H. Plank, and M. Huth, *Nanotechnology* **26**, 475701 (2015).
- ⁴⁰R. Kumar, T. P. I. Unlu, S. Barth, O. Ingólfsson, and D. H. Fairbrother, *J. Phys. Chem. C* **122**, 2648 (2018).
- ⁴¹G. N. Kakazei, P. E. Wigen, K. Y. Guslienko, V. Novosad, A. N. Slavin, V. O. Golub, N. A. Lesnik, and Y. Otani, *Appl. Phys. Lett.* **85**, 443 (2004).
- ⁴²F. Giesen, J. Podbielski, B. Botters, and D. Grundler, *Phys. Rev. B* **75**, 184428 (2007).
- ⁴³H. Schultheiss, S. Schäfer, P. Candeloro, B. Leven, B. Hillebrands, and A. N. Slavin, *Phys. Rev. Lett.* **100**, 047204 (2008).
- ⁴⁴G. De Loubens, A. Riegler, B. Pigeau, F. Lochner, F. Boust, K. Y. Guslienko, H. Hurdequint, L. W. Molenkamp, G. Schmidt, A. N. Slavin, V. S. Tiberkevich, N. Vukadinovic, and O. Klein, *Phys. Rev. Lett.* **102**, 177602 (2009).
- ⁴⁵F. Guo, L. M. Belova, and R. D. McMichael, *Phys. Rev. Lett.* **110**, 017601 (2013).
- ⁴⁶A. Lara, O. V. Dobrovolskiy, J. L. Prieto, M. Huth, and F. G. Aliev, *Appl. Phys. Lett.* **105**, 182402 (2014).
- ⁴⁷X. Zhou, E. V. Tartakovskaya, G. N. Kakazei, and A. O. Adeyeye, *Phys. Rev. B* **96**, 024446 (2017).
- ⁴⁸S. A. Bunyaev, V. O. Golub, O. Y. Salyuk, E. V. Tartakovskaya, N. M. Santos, A. A. Timopheev, N. A. Sobolev, A. A. Serga, A. V. Chumak, B. Hillebrands, and G. N. Kakazei, *Sci. Rep.* **5**, 18480 (2015).
- ⁴⁹A. Vansteenkiste, J. Leliaert, M. Dvornik, M. Helsen, F. Garcia-Sanchez, and B. Van Waeyenberge, *AIP Adv.* **4**, 107133 (2014).
- ⁵⁰M. Tokac, S. A. Bunyaev, G. N. Kakazei, D. S. Schmool, D. Atkinson, and A. T. Hindmarch, *Phys. Rev. Lett.* **115**, 056601 (2015).
- ⁵¹K. Y. Guslienko and A. N. Slavin, *Phys. Rev. B* **72**, 014463 (2005).
- ⁵²Q. Wang, B. Heinz, R. Verba, M. Kewenig, P. Pirro, M. Schneider, T. Meyer, B. Lägél, C. Dubs, T. Brächer, and A. V. Chumak, *Phys. Rev. Lett.* **122**, 247202 (2019).